Conformational Isomerization and Collisional Cooling Dynamics of Bis(2-hydroxyphenyl)methane

Nathan R. Pillsbury, Christian W. Müller, and Timothy S. Zwier*

Department of Chemistry, Purdue University, 560 Oval Drive, West Lafayette, Indiana 47907-2084

Received: November 9, 2008; Revised Manuscript Received: March 3, 2009

Stimulated emission pumping−population transfer spectroscopy (SEP-PTS) has been used to directly measure the energy threshold to isomerization between the two conformational isomers of bis(2-hydroxyphenyl)methane. These conformers have been shown in the preceding paper (DOI 10.1021/jp8098686) to be an OH···O H-bonded structure (conformer A) and a doubly OH ···π H-bonded conformer (conformer B). Lower and upper bounds on the energy threshold for A→B isomerization are at 1344 and 1399 cm^{-1}, respectively, while the corresponding bounds on the B→A isomerization are 1413 and 1467 cm^{-1}. The difference between these thresholds provides a measure of the relative energies of the two minima, with $\Delta E_{AB} = E_A - E_B = 14-123$ cm^{-1}. The transition-state structure responsible for this energy threshold has been identified using DFT B3LYP, DFT M05-2X, and MP2 calculations, all with a 6-31+G* basis set. Only the DFT M05-2X calculations correctly reproduce both the energy ordering of the two minima and the magnitude of the barrier separating them. Below the energy threshold to isomerization, we have used the extensive Franck−Condon progressions present in the SEP spectrum of conformer A to undertake an SEP-PT study of its vibrational relaxation rate, as a function of internal energy over the 0−1200 cm^{-1} region. The position of SEP excitation in the expansion was systematically varied in order to change the rate and number of cooling collisions that occur between SEP excitation and probe steps and the initial temperature at which SEP occurs. From this data set, three energy regimes were identified, each with a unique value of the average energy lost per collision with helium (region 1: 13 cm^{-1}/collision for $E = 300-1200$ cm^{-1}, region 2: 0.6 cm^{-1}/collision for $E = 200-300$ cm^{-1}, and region 3: 7 cm^{-1}/collision for $E < 200$ cm^{-1}). In region 1, the vibrational density of states is sufficient to support efficient loss of energy via $\Delta v = -1$ collisions, involving the lowest-frequency vibrations of the molecule (with a frequency of 26 cm^{-1}). In region 2, the vibrational energy levels are sufficiently sparse that energy gaps exist, reducing the efficiency of relaxation. In region 3, a combination of the quantum nature of the helium, attractive forces, and orbiting resonances may be responsible for the increased efficiency at lowest-energy regime.

I. Introduction

Flexible molecules can have many degrees of freedom that give rise to complicated potential energy surfaces with many conformational minima and a large number of energy barriers separating them. It is often unclear how conformational isomerization proceeds on such surfaces when there may be several pathways that lead from reactant to product. Both experiment and theory typically focus attention on the conformational minima; however, the kinetics and dynamics of conformational isomerization are affected most directly by the energy barriers separating these minima. From a knowledge of the relative energies of the minima and the barrier heights, minimum-energy pathways can be constructed, which will play key roles in the isomerization between the minima of interest. However, it is often difficult to directly determine the barriers to isomerization experimentally, and it is uncertain how well electronic structure calculations model this behavior in larger molecules (∼20−30 atoms). A technique developed in our laboratory called stimulated emission pumping−population transfer spectroscopy (SEP-PTS)[1−7] can be used to directly determine these barriers.

In the preceding paper,[8] the ultraviolet spectroscopy of bis(2-hydroxyphenyl)methane (2HDPM) in a free jet environment was explored in order to lay the groundwork for the experiments described here. 2HDPM has four primary flexible coordinates: two phenyl torsions and two OH torsions. The positions of the OH groups make it possible for them to interact with each other and the other phenyl ring π-cloud, leading to a model 4D potential energy surface. It was determined that two conformers of 2HDPM exist in the jet. Using double-resonance schemes, we have recorded single-conformation infrared and ultraviolet spectra for these two conformers, leading to their assignment to the two structures shown in Figure 1. Conformer A was assigned to the OH···O H-bonded structure, and conformer B was assigned to the OH···π H-bonded structure.

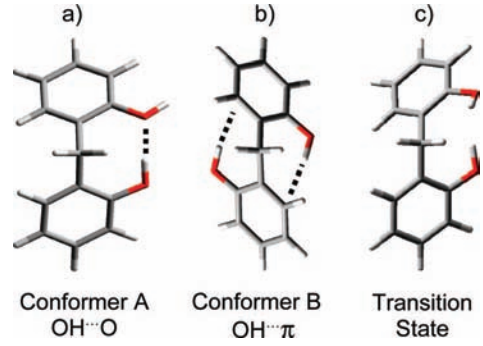

Figure 1. Lowest-energy conformational isomers and calculated transition state of 2HDPM.

* Corresponding author. E-mail: zwier@purdue.edu.

10.1021/jp809870v CCC: $40.75
Published on Web 04/06/2009

In the current study, SEP-PT spectroscopy is used to measure the threshold energies for isomerizing from A→B and B→A. These are intriguing isomerization processes, involving breaking H-bonds of one type and re-forming H-bonds of another. We use the thresholds to place bounds on the barrier to conformational isomerization between these two conformers and to determine the relative energies of the minima. Comparison of the experimental results with theory provides a test of the accuracy of the calculations and leads to insight into the minimum-energy pathway on the multidimensional surface. The SEP-PT methods employed in this work inherently involve measurement of the thresholds to conformational isomerization in competition with vibrational relaxation. In circumstances where we seek to measure these thresholds, our goal is to recool the molecules on as slow a time scale as possible, consistent with repopulation of the zero-point level before interrogation with the probe laser. However, the method is also capable of providing information directly on the vibrational cooling itself.

Studies of collision-induced vibrational energy transfer have a long history.[9−15] With the invention of tunable lasers, it became possible to directly prepare specific vibrational levels and follow vibrational relaxation. Low in the energy manifold, state-to-state propensities can be mapped out using pump−probe methods or by state-resolving the emission from the product levels.[16−23] For large molecules with significant amounts of internal energy, state-to-state studies are no longer possible, but various ingenious methods have been developed to determine the average energy lost per collision as a function of initial internal energy, up to internal energies of 100 kcal/mol or more (35 000 cm^{-1}).[11,15,24,25] From the viewpoint of vibrational energy transfer, 2HDPM is in a class of molecules which has not received much attention previously. As we have already indicated, 2HDPM has two spectroscopically distinguishable minima on a model 4D potential energy surface, involving the phenyl and OH torsions. Several other low-frequency modes, such as the inter-ring bends, also exist adding to the vibrational density of states, leading to state densities of more than 200 states/cm^{-1} at internal energies of only 1000 cm^{-1}. At the same time, such internal energies reach near the top of the barriers to conformational isomerization of interest in 2HDPM.

In the present work, we utilize SEP-PT methods to study vibrational relaxation in the OH···O H-bonded conformer of 2HDPM over the 20−1100 cm^{-1} region. In essence, this method is a variation of that first used by Kable and Knight in their state-to-state single-collision studies that employed SEP excitation.[21] In our case, we follow the recooling back into the "reactant" zero-point level, as a function of the position of SEP excitation in the expansion. In so doing, we give up state-to-state information but extend the initial internal energy into energies near the barriers to conformational isomerization. As we shall see, the results of this study can be used to measure the average energy loss per collision in 2HDPM with helium over internal energies of 0−1100 cm^{-1}. An unusual dependence on internal energy is uncovered that reflects quantum-specific effects as the internal energy is lowered.

II. Experimental Methods

A. SEP Spectroscopy. A total pressure of 3.5 bar of helium was passed through a sample reservoir containing the full vapor pressure of 2HDPM heated to 135 °C. The gaseous sample was then injected into a vacuum chamber (discussed in the preceding paper[8]) via a pulsed valve (General Valve Series 9, 20 Hz) with a 1.2 mm orifice diameter, cooling the molecules to their zero-point vibrational levels (ZPL). At a distance of ∼1 cm from the nozzle orifice, the cooled molecules were excited to the first excited state by a UV laser (pump laser, ∼0.3 mJ/pulse, 20 Hz) fixed at a frequency corresponding to a particular transition in the LIF spectrum (usually the S_0-S_1 origin). Immediately following excitation (∼5−6 ns later), a second UV laser (dump laser, ∼1.5 mJ/pulse, 10 Hz) was used to stimulate emission back to the ground state. When the dump laser is scanned and becomes resonant with an SEP transition, a dip in the total fluorescent signal from the pump laser is detected. In this experiment, the gate of a gated integrator was set between the end of the scattered light signal of the dump laser and the end of the fluorescence tail from the pump laser (a time window of ∼20 ns). Conformation-specific SEP spectra were recorded by plotting the averaged output of the gated integrator (in active baseline subtraction mode) versus the difference in the pump and dump laser frequencies. These spectra were a prerequisite for the SEP-PT experiment.

B. SEP-PTS. SEP-PTS provides a means by which one can experimentally measure the energy thresholds to isomerization between specific reactant−product conformational pairs, even in circumstances where there are many conformers present.[2−6,26] A schematic potential energy diagram for the method is shown in Figure 2a. After initial cooling with helium (∼5−6 bar) to the ZPL, an SEP step is performed early in the supersonic expansion ($x/d \approx 2$; x, distance from nozzle; d, nozzle orifice diameter = 1.2 mm) to put a fraction of the population of a specific conformer into a well-defined S_0 energy level. The frequency of the pump laser (∼0.1−0.3 mJ/pulse, 20 Hz) is fixed on a vibronic band (usually the S_0-S_1 origin) of the reactant conformation. The dump laser (∼0.5−1.0 mJ/pulse, 10 Hz) is scanned, and it stimulates the population down to vibrational levels in the ground state. Then the molecules are given time (∼2 μs) to collisionally recool back to the ZPL where they are probed by a third UV laser (∼0.1−0.2 mJ/pulse, 20 Hz, $x/d \approx 6$). The probe laser can be set to monitor either the reactant or any of the product wells to determine where the population ended up. If the dumped molecules are given an internal energy that is below the barrier to isomerization, then the only place for them to go is back to the ZPL of the reactant well. However, if the energy given is enough to surpass the barrier, then some of the molecules may isomerize and be cooled down to the ZPL of the product well. Because the spectrum is recorded as a difference signal in a 20/10/20 Hz configuration, the recorded output is sensitive only to the population change induced by the dump laser in either the reactant or product population. Thus, in both cases, a gain is observed in the total fluorescence of the probe laser when a transition in the SEP spectrum is encountered by the dump laser. The fluorescence signal from the probe laser is collected as a difference signal using the active baseline subtraction mode of the gated integrator. By tuning the dump laser, one maps out an SEP-PT spectrum for a specific A→B reactant−product pair. Comparing these spectra to the SEP spectra allows for bounds on the barrier to isomerization to be placed. The first SEP transition observed in the SEP-PT spectrum gives an upper bound to the barrier, while the last transition that is not seen gives the lower bound. By measuring the barriers to the forward and reversed reactions between two reactant−product pairs (A→B, B→A), a range on the relative energies of the minima can also be determined.

C. Vibrational Cooling Study. The studies of vibrational cooling employed the same A→A SEP-PT setup, but limited the tuning range of the dump laser to below the A→B isomerization barrier so that only vibrational cooling back into the A zero-point level is possible. A series of measurements

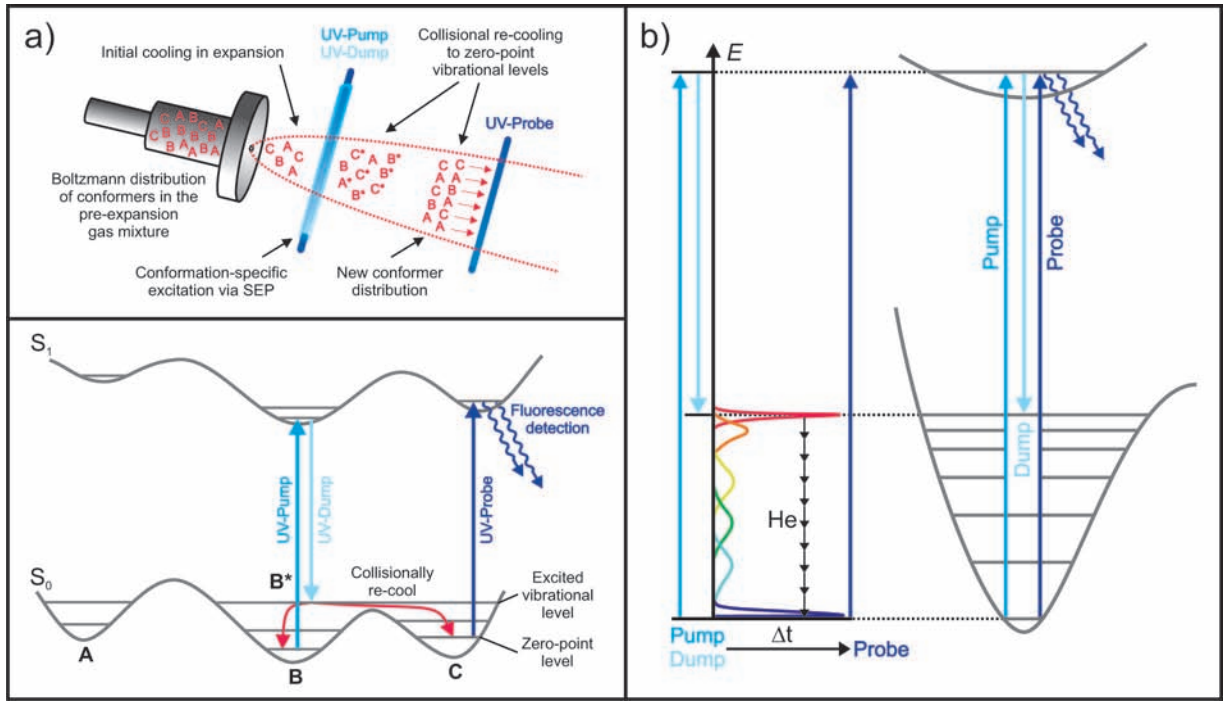

Figure 2. (a) Experimental schematic and potential energy diagram for SEP-PTS. (b) Potential energy diagram for the vibrational cooling experiment, including a representation of the population spread as it cools back down toward the zero-point level.

was carried out in which the position of the valve relative to the lasers was systematically varied. The lasers were kept in the same place in time and space while the nozzle was moved by known distances using a custom-built translation stage to which the pulsed valve was affixed. As the distance between the nozzle orifice and pump/dump lasers was increased, both the collision rate and the total number of collisions with He atoms between the pump/dump and probe steps (about a 2 μs delay) were reduced. In this experiment, a fraction of molecules are excited to the S_1 electronic state, and a fraction of those molecules are stimulated down to a well-defined level in the ground state by the dump laser. Collisions with He atoms generally remove energy in recooling the vibrationally excited molecule, but also lead to a broadening of the (near delta function) initial internal energy spread as cooling proceeds, as shown schematically in Figure 2b. Since the temperatures in the expansion are so low, the population accumulates in the zero-point level while cooling proceeds. By setting the probe laser wavelength on the S_0-S_1 origin of conformer A, the probe signal is sensitive only to the molecules that make it back to the ZPL. Therefore, when there are an insufficient number of collisions to bring the excited molecules back to the ZPL, a decrease in the gain signal from the probe laser is observed.

III. Computational Methods

Calculations of the ground-state conformational minima and the transition state between them were carried out at the B3LYP[27,28]/6-31+G*, M05-2X[29]/6-31+G*, and MP2[30−35]/6-311++G** levels of theory using Gaussian 03.[36] Harmonic vibrational frequencies were also obtained for calculation of the density of states as a function of internal energy in conformer A.

IV. Results and Analysis

A. DFT and ab Initio Calculations. The results of ground-state optimizations of 2HDPM are summarized in Table 1. After zero-point correction, B3LYP/6-31+G* predicts that 2HDPM A is lower in energy than 2HDPM B by 0.69 kcal/mol (~240 cm^{-1}). In contradiction to this, MP2/6-311++G** predicts that 2HDPM B is actually lower in energy by 0.76 kcal/mol (~265 cm^{-1}). The DFT functional of M05-2X yields the same ordering of the minima as MP2 (i.e., 2HDPM B lower than 2HDPM A), but predicts a separation of only 0.5 kcal/mol (~174 cm^{-1}).

TABLE 1: ZPE-Corrected Relative Energies of the Calculated Conformational Minima of 2HDPM at Differing Levels of Theory

level of theory/basis set	relative energy of A (kcal/mol)	relative energy of B (kcal/mol)
B3LYP/6-31+G*	0.00	0.69
MP2/6-311++G**	0.76	0.00
M05-2X/6-31+G*	0.50	0.00

TABLE 2: Predicted and Experimentally Determined Transition-State Energies

	A→B TS energy (cm^{-1})	B→A TS energy (cm^{-1})
B3LYP/6-31+G*	1399	1159
MP2/6-311++G**	563	829
M05-2X/6-31+G*	1185	1359
experiment	1344−1399	1413−1467

Transition-state calculations (QST3) were also performed using the three previously mentioned levels of theory, the results of which are shown in Table 2. The calculated transition state at the B3LYP/6-31+G* level of theory is shown in Figure 1c. All three levels of theory predict this same structure for the transition state between the two conformers. B3LYP predicts the zero-point corrected energy of this structure to be ~1399 cm^{-1} above the zero-point level of 2HDPM A. However, MP2 predicts a barrier less than half of this size (~563 cm^{-1}). Finally, M05-2X/6-31+G* calculations place the zero-point corrected energy of the transition state at 1185 cm^{-1}, a value between the other two, but closer to the B3LYP result. These three levels

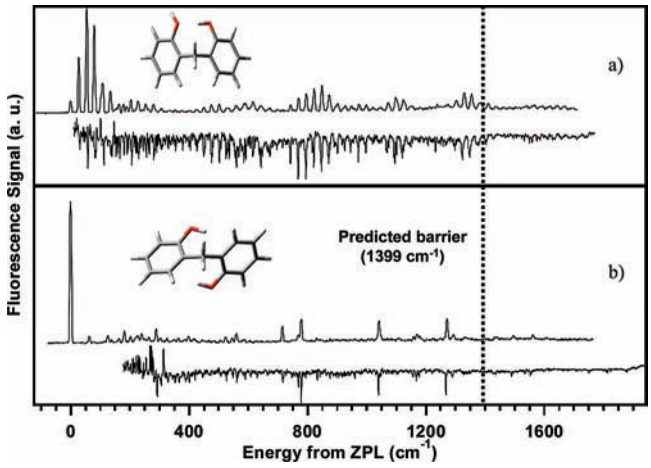

Figure 3. SVLF and SEP spectra of (a) 2HDPMA and (b) 2HDPMB. The dotted line indicates the position of the predicted barrier to isomerization.

of theory can be compared directly with the experimentally determined energy threshold obtained in the next section.

B. SEP-PT Studies of Isomerization. Previously recorded single-vibronic level fluorescence (SVLF) spectra[8] of 2HDPM A and B are shown along with their corresponding SEP spectra in Figure 3a,b. As this figure shows, all of the transitions in the SVLF spectra are observed in SEP, with increased resolution. The ordinate scale is the difference in energy between the pump and dump photons, presented in terms of the internal energy (in cm^{-1}) of the S_0 vibrational level accessed in the downward transition.

The SVLF and SEP spectra of conformer A (Figure 3a) are particularly interesting because they exhibit extensive Franck−Condon (FC) activity in more than 70 transitions that are quite evenly spread over the entire energy range from the zero-point level out to ~1400 cm^{-1}. This FC activity reflects a large change in geometry between the S_1 and S_0 states of 2HDPM A along two low-frequency torsional coordinates.[8] This multitude of transitions provides us with the opportunity to place well-defined amounts of energy into the conformer over a significant energy range. On the other hand, the SVLF and SEP spectra of 2HDPM B (Figure 3b) show very sparse FC activity. The energy predicted for the barrier to isomerization, as predicted by the B3LYP calculations, is shown as a dashed line in Figure 3. This illustrates a particular challenge associated with this experiment since the barrier is predicted to be near the end of the FC-active region, precisely in the region where we anticipate seeing the first evidence for barrier crossing in the SEP-PT spectra.

The SEP and SEP-PT spectra of conformer A over the 800−1700 cm^{-1} energy range are shown in Figure 4. In past SEP-PT studies,[2−6,26] the A→A "reactant" spectrum has shown a decrease in gain signal once the barrier has been overcome due to the fact that population is being split between conformations.[5,26] However, in this study, the A→A spectrum showed no clear evidence for such a reduction, in part because SEP transition intensities are dropping quickly with increasing energy, making it difficult to observe.

The more direct measure of the threshold is contained in the A→B spectrum, which is sensitive to the transfer of population between conformational wells. There we see a clear onset of intensity near 1400 cm^{-1} above the zero-point level of 2HDPM A that indicates that population transfer from A→B is occurring. The asterisks in the upper A→B spectrum at lower energies mark transitions due to A that appear as the result of a very

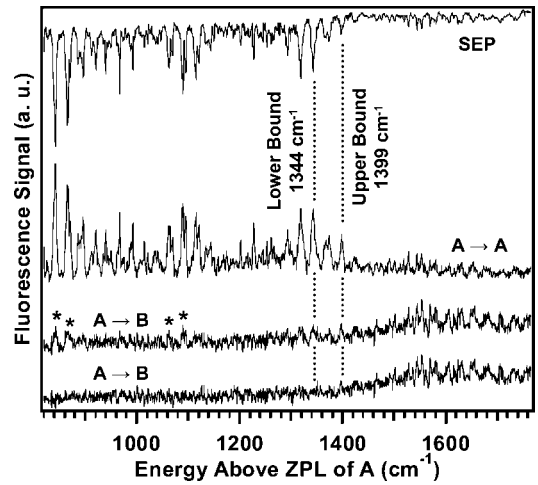

Figure 4. SEP and SEP-PT spectra from 2HDPMA. The dotted lines indicate the upper and lower bounds to the barrier. The transitions marked with asterisks are due to a slight overlap with a vibronic band of 2HDPMA when probing 2HDPMB. This slight contamination has been removed in the bottom trace by subtracting a scaled version of the A→A trace from the A→B trace.

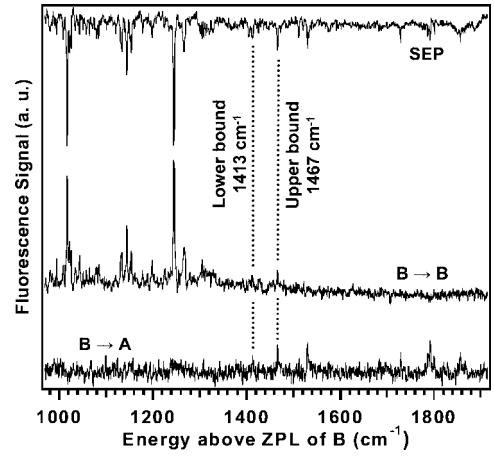

Figure 5. SEP and SEP-PT spectra from 2HDPM B. The dotted lines indicate the upper and lower bounds to the barrier.

minor contamination from a vibronic transition due to A at the wavelength used to probe conformer B (the first vibronic transition of B 22 cm^{-1} above its S_1 origin). This slight contamination has been removed in the bottom trace of Figure 4 by subtracting a scaled version of the A→A spectrum from the A→B spectrum, allowing for the onset of the threshold for A→B isomerization to be observed clearly. The lower and upper bounds of the barrier were determined by noticing that the band at 1344 cm^{-1} in the SEP spectrum is missing in the A→B spectrum, while the band at 1399 cm^{-1} and all subsequent bands in the SEP spectrum are observed. Therefore, we put the lower bound on the barrier to A→B isomerization at 1344 cm^{-1} and the upper bound at 1399 cm^{-1}. These bounds are depicted as dashed lines in Figure 4. In addition, the A→B SEP-PT spectrum shows a gradual increase in gain that stretches from 1400 to 1550 cm^{-1}. This gradual onset appears because the SEP spectrum in this region is a dense manifold of ground-state levels that can support SEP at all wavelengths in this threshold region.

The SEP and SEP-PT spectra out of 2HDPM B are shown in Figure 5. In this case the B→B spectrum was helpful because an abrupt decrease in intensity was seen above 1460 cm^{-1}. In fact, the last band observed in this spectrum is at 1467 cm^{-1}, above the zero-point level of B. The first transition seen in the

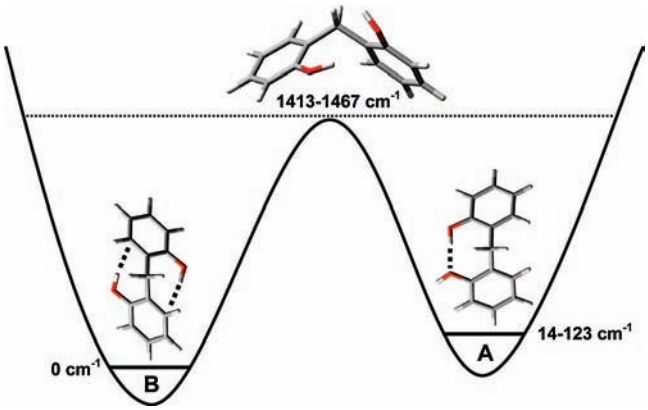

Figure 6. 1D representation of the ground-state potential energy surface for 2HDPM with the experimental measurements included.

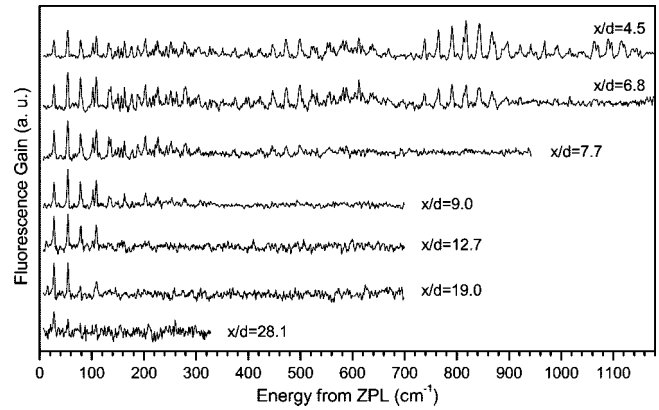

Figure 7. SEP-PT spectra of A→A recorded at the indicated distances (in nozzle diameters, *d*) between the nozzle orifice and the position of SEP excitation.

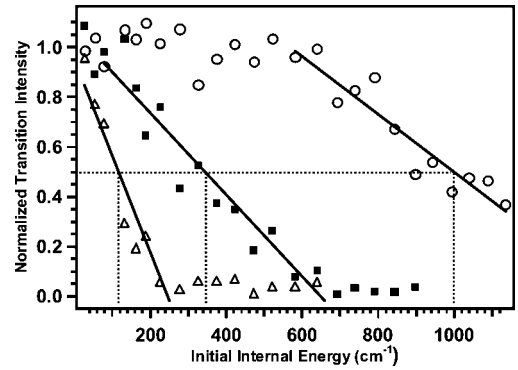

Figure 8. Representative plots of normalized transition intensity versus initial internal energy at *x*/*d* values of 5.9 (open circles), 7.7 (filled squares), and 14.5 (open triangles). The dotted lines indicate the amount of internal energy at which 50% of the population is being cooled to the zero-point level at each *x*/*d* position.

B→A spectrum also occurs at 1467 cm^{-1} with all bands above it visible. By comparing with the intensities in the SEP spectrum, the last band that is not observed in the B→A spectrum is at 1413 cm^{-1}. Therefore, we place the lower bound of the barrier of B→A at 1413 cm^{-1} and the upper bound at 1467 cm^{-1} as indicated by the dashed lines in Figure 5. Because the A→B and B→A thresholds involve the same energy barrier, they can be combined to provide a measure of the energy difference between the zero-point levels of conformers A and B. That is,

$$E_{\text{thresh}}(\text{B}\rightarrow\text{A}) = E(\text{barrier}) - E_{\text{B}} = 1413 - 1467\ \text{cm}^{-1}$$

$$E_{\text{thresh}}(\text{A}\rightarrow\text{B}) = E(\text{barrier}) - E_{\text{A}} = 1344 - 1399\ \text{cm}^{-1}$$

$$E_{\text{thresh}}(\text{B}\rightarrow\text{A}) - E_{\text{thresh}}(\text{A}\rightarrow\text{B}) = E_{\text{A}} - E_{\text{B}} = \Delta E_{\text{AB}} = 14 - 123\ \text{cm}^{-1}$$

Thus, our measurements indicate that the zero-point energy of conformer A is 14−123 cm^{-1} above that for conformer B, indicating that conformer B is in fact the global minimum. A schematic energy diagram that summarizes the experimental results is shown in Figure 6.

C. SEP-PT Studies of Vibrational Cooling. This study was made possible because of the long FC progressions noted earlier in the SEP spectrum of conformer A. It utilizes the full triple-resonance SEP-PT technique in an attempt to get an average value for the amount of energy removed per collision with helium as a function of the internal energy of 2HDPM A. A total of 32 A→A SEP-PT scans were recorded with the SEP step carried out at a range of distances from the throat of the nozzle. These distances are reported in terms of *x*/*d*, the number of nozzle diameters (d = 1.2 mm), with values ranging from ∼3 to 28. This distance was measured by setting zero as the position at which half of the SEP pump laser beam was blocked by the nozzle face plate, using the known thread pitch for the z translation stage. Figure 7 shows seven selected spectra taken at several *x*/*d* values in this range. Each trace is an average of two spectra. The top trace (x/d = 4.5) is taken under optimal conditions for A→A gain, and all transitions are observed. The second trace (x/d = 6.8) shows that some of the high-frequency bands are either smaller than those in the top trace or missing entirely. These bands are missing because at the indicated *x*/*d* position, there are no longer enough collisions with helium to cool the molecules back to the ZPL from those energies. As the *x*/*d* value is increased, more and more bands disappear because there are simply not enough collisions to remove all of the energy given to the molecules.

Our goal is to use our data to determine the average energy lost per collision by 2HDPM A as a function of internal energy E_{int}. After normalization to the x/d = 3 data (in which cooling is complete for all levels considered), the intensity of selected SEP-PT transitions was measured as a function of *x*/*d*. A set of representative plots of this type based on data from the x/d = 5.9, 7.7, and 14.5 scans is shown in Figure 8. In principle, each plot can be used to determine the width and shape of the distribution of population as it arrives at the ZPL as a function of initial internal energy, as shown schematically in Figure 2b. We expect these plots to be sigmoidal in shape, with the 50% point being a sensitive function of the initial internal energy and *x*/*d* position. Given the scatter in the data, we choose instead to use each plot at a given *x*/*d* value simply to determine the internal energy at which 50% of the population returns to the zero-point level under those cooling conditions. For that purpose, we carry out a linear least-squares fit to the near-linear portion of the sigmoidal curve. Since the family of curves in Figure 8 is determined by changing the nozzle-SEP distance, while maintaining a constant time delay between SEP and probe steps (2 μs), we thereby effectively vary the number of 2HDPM collisions with helium during the traversal of the molecules between the pump/dump and probe lasers. The single-molecule collision rate z_{jet} (collisions/sec) experienced by 2HDPM at a given *x*/*d* position with the helium atoms used as buffer gas can be estimated, using a modified version of the formula from

Lubman et al. for a free jet expansion modeled as an isentropic continuum ideal gas flow:[37,38]

$$z_{\text{jet}} = n_0 \sigma^{\text{red}} \bar{v}_0 \left[1 + \frac{1}{2}(\gamma - 1) M_{\text{eff}}^2\right]^{-\frac{1}{2}\left[\frac{\gamma+1}{\gamma-1}\right]} \quad (1)$$

In eq 1, n_0 is the reservoir density of He, σ^{red} is the collision cross section for He-2HDPM collisions, $\bar{v}_0$ is the mean velocity in the reservoir, γ is the heat capacity ratio C_p/C_v for He (5/3), and M_{eff} is the local Mach number at position x/d in the jet.

We have calculated σ^{red} assuming two different models for the collision cross section. In the simplest case, σ^{red} is approximated as a hard-sphere cross section for 2HDPM-He collisions, with $d = {}^1/_2(d_{\text{2HDPM}} + d_{\text{He}})$, which for $d_{\text{2HDPM}} = 8.0$ Å and $d_{\text{He}} = 2.7$ Å gives $\sigma^{\text{red}}_{\text{HS}} = \pi \cdot d^2/4 = 50$ Å^2. In order to take into account the quantum nature of the He atom at low temperatures, a second calculation was used, $d_{\text{He}} = \lambda_{\text{He}} = h/m\upsilon_{\text{rel}}$,when $\lambda_{\text{He}} > 2.7$ Å and $\upsilon_{\text{rel}}(x)$ is the relative velocity of 2HDPM-He collisions at position x and translational temperature $T(x)$. Based on the time delay between SEP and probe lasers (2 μs), the position of the probe laser beam x_{probe} relative to the position of SEP excitation (x_{SEP}) was determined by numerical integration of $x/\upsilon(x)$ where $\upsilon(x)$ is the mean mass flow velocity.[39] The number of collisions between SEP and probe steps was calculated by numerically integrating $z(x)(x/\upsilon(x))$.

Figure 9 shows plots of the initial internal energy at which 50% of the population reaches the zero-point level $E_{\text{int}}(P_{50})$ versus the number of collisions estimated. Both plots divide into three regions, each with its own near-linear slope. In the hard sphere case, these regions span the 0−25, 25−50, and 50−120 collision range with slopes of 7.7, 0, and 13.2 cm^{-1}/hard-sphere collision. The effect of the quantum nature of He is to increase the number of collisions at low temperatures, thereby reducing the slopes to 4.5, 0, and 11.3 cm^{-1}/collision. We will consider the reasons behind these three regimes in more detail in the Discussion section.

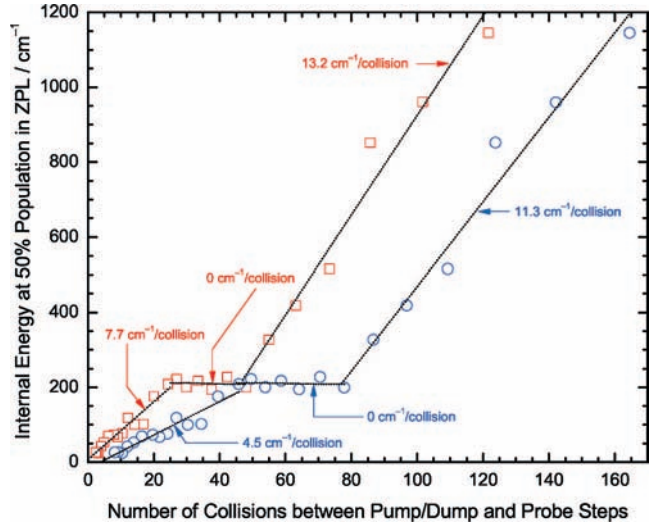

Figure 9. Plot of the internal energy at which 50% of the population is cooled back to the zero-point level versus the calculated number of collisions experienced between the SEP and probe steps, assuming hard-sphere collisions (□) or taking the quantum nature of He into account (○). See text for further discussion. Linear fits are labeled with their respective slopes in cm^{-1}/collision.

V. Discussion

A. SEP-PT Study. We have experimentally put relatively narrow bounds on the energy threshold to isomerization between conformers A and B of 2HDPM. The threshold from A to B was determined to lie between 1344 and 1399 cm^{-1}, while that from B to A was between 1413 and 1467 cm^{-1}. By taking the difference in these threshold values, we also obtained the relative energies of the two minima, with $\Delta E_{\text{AB}} = E_{\text{A}} - E_{\text{B}} = 14-123$ cm^{-1}. Thus, conformer B is 14−123 cm^{-1} lower in energy than conformer A.

Predicted and experimentally determined TS energies are shown in Table 2. These two conformers have remarkably similar energy stabilities, but quite different modes of stabilization (e.g., one OH···O H-bond versus two OH···π H-bonds). The previously recorded LIF and UVHB showed that the two conformers had similar intensities, suggesting that they were similar in energy. Our SEP-PTS results now confirm that notion and quantify the difference. However, it is difficult to quantify the relative populations because the two conformers have such different FC factors and they also could differ in their inherent oscillator strengths, so the relationship between intensity and population is not straightforward.

The SEP-PT results also serve as a test of the accuracy of theoretical methods. Current standard computational methods have certain limitations when it comes to dispersion forces and hydrogen bonding. It is well known that the density functional theory (DFT) employing a standard functional such as B3LYP does not account for dispersion forces correctly and systematically underestimates them, while MP2 calculations inherently suffer from intramolecular BSSE, except when very large basis sets are employed, and also tend to systematically overestimate dispersion.[40,41] There have been several corrections made to DFT calculations in order to correct its deficiencies. One notable recent attempt was the new functional introduced by Truhlar and co-workers, called M05-2X.[29,42,43] In systems where dispersion and hydrogen bonding play a significant role, this method has been found to outperform both B3LYP and MP2.[29,42,43] Looking back at Table 1, we can now test the three levels of theory for accuracy. The B3LYP results predict that 2HDPM A is lower in energy than 2HDPM B by 0.69 kcal/mol (~240 cm^{-1}), but correctly predict the energy of the transition state (Table 2). The slightly higher predicted energy of 2HDPM B is consistent with B3LYP underestimating dispersive interactions, since the conformer clearly has significant dispersive interactions between the hydroxyl groups and the π-clouds of the rings. As for MP2, it correctly orders the relative energies of the two minima, but as shown by Table 2 predicts the isomerization barrier to be much lower (~830 cm^{-1}) than the experimental value (~1400 cm^{-1}). M05-2X was the only method of the three studied to correctly predict both the relative energies of the minima and the height of the barrier between them. This result provides further evidence that the M05-2X functional does successfully provide a better account of dispersive interactions and hydrogen bonding.

Though B3LYP, MP2, and M05-2X all give different results for the energies of the minima and transition state, the predicted minimum-energy geometries for the two conformers of 2HDPM are very close to one another. The key structural parameters are given in the preceeding paper.[8] The predicted structure of the transition state (Figure 6) is important because it provides some insight into the nature of the isomerization pathway. This structure shows the acceptor OH group from 2HDPM A has rotated around by almost 180°, thereby breaking the OH···O H-bond. In doing so, the "donor" OH is able to slide underneath the opposing phenyl ring, forming an OH···π H-bond. This single OH···π H-bond provides stabilization that partially

counteracts the destabilization associated with loss of the initial OH···O H-bond. Nudged elastic band calculations recently proved to be useful for determining the minimum-energy pathway in the shuttling of a water molecule between two H-bonding sites of *trans*-formanilide.[5] Due to the large geometry changes involved in the isomerization of 2HDPM, these calculations may also be helpful to follow the minimum-energy pathway between A and B.

B. Vibrational Cooling Study. The second major aspect of the present study was the study of vibrational relaxation, which utilized the long Franck−Condon progressions in 2HDPM A that extend to energies about 1200 cm^{-1} above the S_0 zero-point level, very near the barrier to isomerization. The rich data set illustrated in Figure 7 was used to extract the distances from the nozzle at which 50% of the population of 2HDPM A, initially excited to a given internal energy, was returned to the zero-point level by collisional cooling. Using calculated values of the collision rate with helium as a function of *x*/*d*, it was possible to extract from the data the plot shown in Figure 9 of the internal energy at which 50% of the population was returned to the zero-point level versus the number of collisions occurring between the pump/dump (SEP) and probe steps.

As noted earlier, the plots in Figure 9 show three different cooling regimes, each characterized by a linear segment of the plot. The slopes of these segments are a measure of the average internal energy lost per collision in those portions of the expansion. It is important to note that the data set used to create Figure 9 has as its variable parameter the *x*/*d* position at which the SEP step is carried out. Variations in *x*/*d* change not only the number of collisions between SEP and probe steps, but also the initial temperature in the expansion, which affects the 2HDPM-He relative velocity distribution. At small values of *x*/*d* ranging from 5to 8, the 2HDPM molecules experience some 120−50 collisions with helium between the SEP and probe steps, with the initial expansion temperature varying from 9 to 5 K. The slope of the plot over initial internal energies in the 300−1100 cm^{-1} range indicates that approximately 13 cm^{-1} of energy is removed per collision with helium. We note that the density of states varies from 1to 230 states/cm^{-1} over this energy range. This density of states is dominated by the lowest frequency modes in 2HDPM, the ring torsions. We hypothesize that $\Delta v(T) = -1$ transitions involving the lowest-frequency torsional mode (symmetric ring torsion *T* with frequency 27 cm^{-1}) are the dominant vibrational relaxation pathways in this energy range. This is consistent with previous studies of vibrational energy transfer in large molecules.[44−46] If such transitions occurred with unit efficiency, then the slope would be 27 cm^{-1}/collision. The observed slope, then, is equivalent to a $\Delta v(T) = -1$ transition occurring with roughly 50% efficiency.

The second regime is at *x*/*d* values between 8 and 11, where there are between 50 and 30 collisions between SEP and probe steps, occurring at temperatures in the 5−2 K range. For 2HDPM molecules with about 200 cm^{-1} of internal energy, the collisions in this part of the expansion are far less efficient than those of the higher-energy region, with a slope near zero. As Figure 10 shows, the known frequencies of the low-frequency vibrations can be used to calculate the vibrational energy levels present in the first 300 cm^{-1} of 2HDPM A. At higher energies, the near continuum of energy levels makes it possible to follow a succession of $\Delta v(T) = -1$ collisions from any initial energy. However, at lower energies, there are significant energy gaps that must be traversed during the cooling process, reducing the efficiency of the collisions. The sparse nature of the energy level

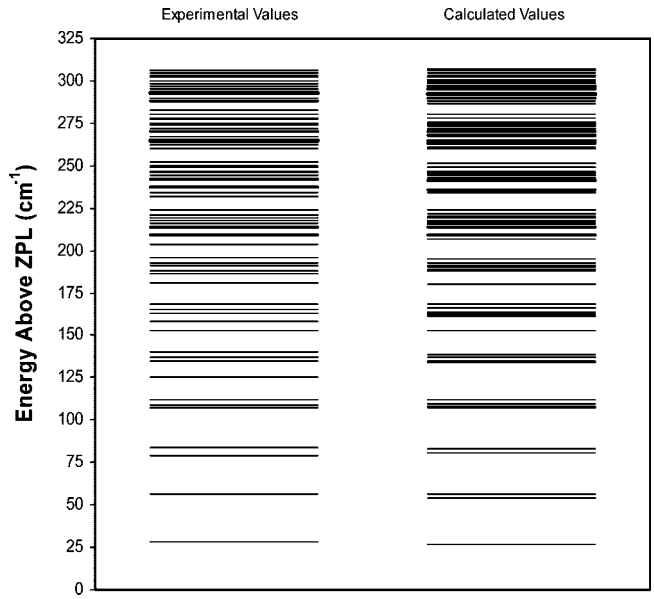

Figure 10. Energy level diagrams for 2HDPM A constructed from experimental and calculated vibrational frequencies.

structure also means that some of the populated levels will have $v(T) = 0$, which will be deactivated less efficiently (see Table 1 of preceding paper[8] for ground-state frequencies). There may also be a decrease in efficiency caused by the colder temperatures at which the collisions occur.

Finally, at the largest *x*/*d* values (12−28), the translational temperatures drop still further into the 0.2−2 K range, where we estimate that just a few hard-sphere collisions (1−25) would occur between SEP and probe steps. Here, there is an increase in per collision efficiency again, with a slope to the plot of ∼8 cm^{-1}/collision. Initially, this is quite surprising since in this lowest energy region (<200 cm^{-1}), just a few pathways are available for relaxation involving well-defined energy levels. We cannot identify with certainty the cause of this increased efficiency. However, three contributions are expected to increase the collision cross section at these lowest temperatures beyond the hard-sphere limit. First, given helium's small mass, at low temperatures its quantum behavior becomes significant. For example, at $T = 1$ K, helium's quantum wavelength ($\lambda = h/p$) is 12 Å, a value slightly larger than the hard-sphere diameter of 2HDPM (∼8 Å). This motivated a model which included the effect, leading to the second curve (in blue circles) in Figure 9. However, the increase in collision cross section is a smooth function that changes the slope but not the overall shape. Second, at these low relative velocities ($v_{He} = 70$ m/s), the weak Lennard-Jones attractive forces between helium and 2HDPM A have sufficient time to affect the intermolecular trajectory and increase the collision cross section. Previous studies have quantified this latter effect.[17,38,47] However, we would not expect this effect either to change the three-regime behavior observed. Third, it is possible that the increased efficiency results from a resonance enhancement of the vibrational energy relaxation. Several previous theoretical studies have predicted the presence of these orbiting resonances,[18,44,48,49] which increase the efficiency of vibrational relaxation by increasing the duration of the collision as the collision energy becomes small (<10 cm^{-1}). There are also several experimental studies that report evidence for these resonance effects.[50−53] However, there are also many studies that have been able to explain the enhancement of the vibrational cooling using simply a Lennard-Jones collision model.[17,38,47] Though they found no experimental evidence of

resonances, they could not rule out the possibility of their existence. Finally, the unusual concave shape of 2HDPM may facilitate multiple-encounter collisions. In order to account for this effect quantitatively, modeling that takes into account the molecular shape explicitly would be required. In fact, the modeling of hard-sphere scattering of large molecules by Shvartsburg et al.[54] indicates that cup-shaped molecules, to which 2HDPM bears a resemblance, are particularly poorly modeled as simple spheres. This is an unexplored avenue left for future work. In the end, the present study cannot distinguish between resonance enhancement and molecular shape effects as the source of the increased collision efficiency at the lowest temperatures, and, in fact, both may contribute.

C. Effect of Vibrational Relaxation on the Isomerization Thresholds. The experimental barrier can also be used to test the rate of isomerization predicted by the Rice−Ramsperger−Kassel−Marcus (RRKM) theory.[55,56] In order for efficient isomerization to take place, the rate of isomerization must be significantly faster than the collision rate. Using the calculated vibrational frequencies for 2HDPM A, the RRKM prediction for the rate of isomerization from A to B at threshold (i.e., when there is a single transition-state level accessible) is $k_{isom}(1350\ cm^{-1}) = \sim 4 \times 10^7\ s^{-1}$. By comparison, the rate of collisions (k_{coll}) at an $x/d = 2$ for an expansion with backing pressure of $P_0 = 6$ bar helium is estimated to be $\sim 8 \times 10^8$ collisions/s.[37] Using the calculated vibrational frequencies of the A↔B transition state, we estimate that $k_{isom} = k_{coll} \sim 250\ cm^{-1}$ above the isomerization barrier. However, based on the known vibrational cooling rate in this energy region (with an average loss of 13 cm^{-1} per hard-sphere collision with helium), starting from this energy, isomerization will be complete (>95%) before vibrational cooling has brought the energy below the isomerization threshold. If we conservatively assume that the gain signal into the product well will be detectable if 50%, then the kinetic shift is reduced to about 100 cm^{-1}.

This estimate for the energy range over which the competition between isomerization and vibrational cooling is observed is consistent with the gradual onset in intensity observed in the A→B spectrum shown in Figure 4. The band at 1399 cm^{-1} is barely visible above the noise, and the intensity of the dense background of states that follow grows in over ~150 cm^{-1} to the full intensity observed in the SEP spectrum. Therefore, in 2HDPM, the signal-to-noise ratio is sufficiently good that we are able to observe the true threshold to isomerization and the competition with cooling, without a sizable kinetic shift. It is also unlikely that tunneling is playing a significant role in the isomerization since the motion of two heavy aromatic rings is involved here.

VI. Conclusions

We have experimentally measured the barrier to isomerization between the two observed conformations of 2HDPM using stimulated emission pumping−population transfer spectroscopy. By measuring the barriers of the forward and reverse reactions, the relative energies of the minima were also obtained. These measurements provided a direct experimental test of DFT B3LYP, MP2, and DFT M05-2X methods. The former two methods suffer from systematic deficiencies and poorly describe either the relative energies of the minima (B3LYP) or the barrier heights (MP2). We established that the DFT functional of M05-2X correctly predicted both of these aspects of the potential energy surface.

A study of the collision-induced vibrational energy relaxation of conformer A was also undertaken. Analysis of these data set led to a measurement of the average energy lost per collision with helium in 2HDPM A over the energy range from 0 to 1100 cm^{-1} internal energy. This data set is unique in probing a large, flexible molecule with many low-frequency vibrations below 200 cm^{-1}. Three distinct energy regimes were observed, with slopes of 13 (300−1100 cm^{-1}), <1 (200−300 cm^{-1}), and 7 cm^{-1}/collision (<200 cm^{-1}). The presence of such low-frequency vibrations leads to a fast increase in the density of states, so that already at 300 cm^{-1} internal energy there is approximately 1 state/cm^{-1}, and by 1100 cm^{-1} there are 200 states/cm^{-1}. We propose that collisions with helium are quite efficient in removing one quantum of the lowest frequency vibration of 2HDPM, ~25 cm^{-1}. Between 200 and 300 cm^{-1}, larger energy gaps decrease the efficiency of vibrational relaxation. Finally, at the lowest energies and lowest temperatures, the enhancement of the cooling rate could arise from the action of weak helium-2HDPM attractions, an increased helium collision cross section due to its quantum nature, or orbiting resonances.

Acknowledgment. This work was supported by the Department of Energy Basic Energy Sciences, Division of Chemical Sciences under Grant No. DE-FG02-96ER14656. This work was also supported in part by a fellowship from Merck Research Laboratories. GridChem (http:www.gridchem.org)[57] is acknowledged for computational resources and services for the selected results used in this publication. N.R.P. acknowledges Purdue University and the Andrews family for the Frederick N. Andrews Fellowship. C.W.M. thanks the "Deutsche Akademie der Naturforscher Leopoldina" for a postdoctoral scholarship (grant number BMBF-LPD 9901/8-159 of the "Bundesministerium für Bildung und Forschung").

References and Notes

(1) Zwier, T. S. *J. Phys. Chem. A* **2006**, *110*, 4133.
(2) Dian, B. C.; Clarkson, J. R.; Zwier, T. S. *Science* **2004**, *303*, 1169.
(3) Clarkson, J. R.; Baquero, E.; Zwier, T. S. *J. Chem. Phys.* **2005**, *122*, 214312.
(4) Clarkson, J. R.; Dian, B. C.; Moriggi, L.; DeFusco, A.; McCarthy, V.; Jordan, K. D.; Zwier, T. S. *J. Chem. Phys.* **2005**, *122*, 214311.
(5) Clarkson, J. R.; Baquero, E.; Shubert, V. A.; Myshakin, E. M.; Jordan, K. D.; Zwier, T. S. *Science* **2005**, *307*, 1443.
(6) Selby, T. M.; Clarkson, J. R.; Mitchell, D.; Fitzpatrick, J. A. J.; Lee, H. D.; Pratt, D. W.; Zwier, T. S. *J. Phys. Chem. A* **2005**, *109*, 4484.
(7) Selby, T. M.; Zwier, T. S. *J. Phys. Chem. A* **2005**, *109*, 8487.
(8) Pillsbury, N. R.; Müller, C. W.; Plusquellic, D. F.; Meerts, W. L.; Zwier, T. S. *J. Phys. Chem. A* **2008**, DOI 10.021/jp8098686.
(9) Cottrell, T. L.; McCoubrey, J. C. *Molecular Energy Transfer in Gases*; Butterworths: London, 1961.
(10) Moore, C. B. *Annu. Rev. Phys. Chem.* **2007**, *58*, 1.
(11) Flynn, G. W.; Parmenter, C. S.; Wodtke, A. M. *J. Phys. Chem.* **1996**, *100*, 12817.
(12) Nikitin, E. E.; Troe, J. *Phys. Chem. Chem. Phys.* **2008**, *10*, 1483.
(13) Silva, M.; Jongma, R.; Field, R. W.; Wodtke, A. M. *Annu. Rev. Phys. Chem.* **2001**, *52*, 811.
(14) Barker, J. R.; Yoder, L. M.; King, K. D. *J. Phys. Chem. A* **2001**, *105*, 796.
(15) Yuan, L. W.; Du, J.; Mullin, A. S. *J. Chem. Phys.* **2008**, 129.
(16) Leone, S. R. *J. Phys. Chem. Ref. Data* **1982**, *11*, 953.
(17) Muller, D. J.; McKay, R. I.; Edwards, G. B.; Lawrance, W. D.; Hardy, J. P.; Rock, A. B.; Selway, K. J.; Kable, S. H.; Knight, A. E. W. *J. Phys. Chem.* **1988**, *92*, 3751.
(18) Villarreal, P.; Delgadobarrio, G.; Mareca, P. *J. Chem. Phys.* **1982**, *76*, 4445.
(19) Krajnovich, D. J.; Parmenter, C. S.; Catlett, D. L. *Chem. Rev.* **1987**, *87*, 237.
(20) Orr, B. J. *Int. Rev. Phys. Chem.* **2006**, *25*, 655.
(21) Kable, S. H.; Knight, A. E. W. *J. Chem. Phys.* **1990**, *93*, 3151.
(22) Waclawik, E. R.; Lawrance, W. D. *J. Phys. Chem. A* **2003**, *107*, 10507.
(23) Rainbird, M. W.; Webb, B. S.; Knight, A. E. W. *J. Chem. Phys.* **1988**, *88*, 2416.
(24) Frerichs, H.; Hollerbach, M.; Lenzer, T.; Luther, K. *J. Phys. Chem. A* **2006**, *110*, 3179.

(25) Park, J.; Shum, L.; Lemoff, A. S.; Werner, K.; Mullin, A. S. *J. Chem. Phys.* **2002**, *117*, 5221.
(26) Selby, T. M.; Zwier, T. S. *J. Phys. Chem. A* **2007**, *111*, 3710.
(27) Becke, A. D. *Phys. Rev. A* **1988**, *38*, 3098.
(28) Lee, C. T.; Yang, W. T.; Parr, R. G. *Phys. Rev. B* **1988**, *37*, 785.
(29) Zhao, Y.; Schultz, N. E.; Truhlar, D. G. *J. Chem. Theory Comput.* **2006**, *2*, 364.
(30) Frisch, M. J.; Headgordon, M.; Pople, J. A. *Chem. Phys. Lett.* **1990**, *166*, 275.
(31) Frisch, M. J.; Headgordon, M.; Pople, J. A. *Chem. Phys. Lett.* **1990**, *166*, 281.
(32) Headgordon, M.; Headgordon, T. *Chem. Phys. Lett.* **1994**, *220*, 122.
(33) Headgordon, M.; Pople, J. A.; Frisch, M. J. *Chem. Phys. Lett.* **1988**, *153*, 503.
(34) Moller, C.; Plesset, M. S. *Phys. Rev.* **1934**, *46*, 0618.
(35) Saebo, S.; Almlof, J. *Chem. Phys. Lett.* **1989**, *154*, 83.
(36) Frisch, M. J.; Trucks, G. W.; Schlegel, H. B.; Scuseria, G. E.; Robb, M. A.; Cheeseman, J. R.; Montgomery, J. A.; Jr., T. V.; Kudin, K. N.; Burant, J. C.; Millam, J. M.; Iyengar, S. S.; Tomasi, J.; Barone, V.; Mennucci, B.; Cossi, M.; Scalmani, G.; Rega, N.; Petersson, G. A.; Nakatsuji, H.; Hada, M.; Ehara, M.; Toyota, K.; Fukuda, R.; Hasegawa, J.; Ishida, M.; Nakajima, T.; Honda, Y.; Kitao, O.; Nakai, H.; Klene, M.; Li, X.; Knox, J. E.; Hratchian, H. P.; Cross, J. B.; Bakken, V.; Adamo, C.; Jaramillo, J.; Gomperts, R.; Stratmann, R. E.; Yazyev, O.; Austin, A. J.; Cammi, R.; Pomelli, C.; Ochterski, J. W.; Ayala, P. Y.; Morokuma, K.; Voth, G. A.; Salvador, P.; Dannenberg, J. J.; Zakrzewski, V. G.; Dapprich, S.; Daniels, A. D.; Strain, M. C.; Farkas, O.; Malick, D. K.; Rabuck, A. D.; Raghavachari, K.; Foresman, J. B.; Ortiz, J. V.; Cui, Q.; Baboul, A. G.; Clifford, S.; Cioslowski, J.; Stefanov, B. B.; Liu, G.; Liashenko, A.; Piskorz, P.; Komaromi, I.; Martin, R. L.; Fox, D. J.; Keith, T.; Al-Laham, M. A.; Peng, C. Y.; Nanayakkara, A.; Challacombe, M.; Gill, P. M. W.; Johnson, B.; Chen, W.; Wong, M. W.; Gonzalez, C.; Pople, J. A. *Gaussian 03, Revision E.01*; Gaussian, Inc.: Wallingford CT, 2004.
(37) Lubman, D. M.; Rettner, C. T.; Zare, R. N. *J. Phys. Chem.* **1982**, *86*, 1129.
(38) Darr, J. P.; Loomis, R. A. *Phys. Chem. Chem. Phys.* **2005**, *7*, 3323.
(39) Scoles, G. *Atomic and Molecular Beam Methods*; Oxford University Press: New York, 1988; Vol. 1.
(40) Holroyd, L. F.; van Mourik, T. *Chem. Phys. Lett.* **2007**, *442*, 42.
(41) Shields, A. E.; van Mourik, T. *J. Phys. Chem. A* **2007**, *111*, 13272.
(42) Zhao, Y.; Truhlar, D. G. *J. Chem. Theory Comput.* **2007**, *3*, 289.
(43) Zhao, Y.; Truhlar, D. G. *Acc. Chem. Res.* **2008**, *41*, 157.
(44) Rice, S. A. *J. Phys. Chem.* **1986**, *90*, 3063.
(45) Pursell, C. J.; Parmenter, C. S. *J. Phys. Chem.* **1993**, *97*, 1615.
(46) Stone, T. A.; Parmenter, C. S. *J. Phys. Chem. A* **2002**, *106*, 938.
(47) Rock, A. B.; Vanzoeren, C. M.; Kable, S. H.; Edwards, G. B.; Knight, A. E. W. *J. Chem. Phys.* **1988**, *89*, 6777.
(48) Cerjan, C.; Rice, S. A. *J. Chem. Phys.* **1983**, *78*, 4952.
(49) Gray, S. K.; Rice, S. A. *J. Chem. Phys.* **1985**, *83*, 2818.
(50) Cabanillas-Vidosa, I.; Pino, G. A.; Rinaldi, C. A.; Ferrero, J. C. *Chem. Phys. Lett.* **2006**, *429*, 27.
(51) Jouvet, C.; Sulkes, M.; Rice, S. A. *Chem. Phys. Lett.* **1981**, *84*, 241.
(52) Kroes, G. J.; Dateo, C. E.; Clary, D. C. *Chem. Phys.* **1990**, *140*, 255.
(53) Sulkes, M.; Tusa, J.; Rice, S. A. *J. Chem. Phys.* **1980**, *72*, 5733.
(54) Shvartsburg, A. A.; Jarrold, M. F. *Chem. Phys. Lett.* **1996**, *261*, 86.
(55) Baer, T.; Hase, W. L. *Unimolecular Reaction Dynamics: Theory and Experiments*; Oxford University Press: Oxford, 1996.
(56) Marcus, R. A. *J. Chem. Phys.* **1952**, *20*, 359.
(57) Dooley, R. A.; Pamidighantam, S. *Computational Chemistry Grid: Production Cyberinfrastructure for Computational Chemistry*, Proceedings of the 13th Annual Mardi Gras Conference; Louisiana State University, Baton Rouge, LA, 2005.

JP809870V